Supplementary information

Interaction Driven Giant Electrostatic Modulation of Ion Permeation in Atomically Small Capillaries

Dhal Biswabhusan[1], Yechan Noh[3], Sanat Nalini Paltasingh[4], Chandrakar Naman[1], Siva Sankar Nemala[5], Rathi Aparna[1], Kaushik Suvigya[1], Andrea Capasso[5], Saroj Kumar Nayak[3], Li-Hsien Yeh[6,7,8], Kalon Gopinadhan*[1,2]

[1]Department of Physics, Indian Institute of Technology Gandhinagar, Gujarat 382355, India

[2]Department of Materials Engineering, Indian Institute of Technology Gandhinagar, Gujarat 382355, India

[3]Department of Physics, University of colorado Boulder, Boulder, CO 80309, USA

[4]School of Basic Sciences, Indian Institute of Technology Bhubaneswar, Khorda, Odisha-752050, India

[5]International Iberian Nanotechnology Laboratory, Braga 4715-330, Portugal

[6]Department of Chemical Engineering, National Taiwan University of Science and Technology, Taipei 10607, Taiwan

[7]Graduate Institute of Energy and Sustainability Technology, National Taiwan University of Science and Technology, Taipei 10607, Taiwan

[8]Advanced Manufacturing Research Center, National Taiwan University of Science and Technology, Taipei 10607, Taiwan

(*Corresponding author Email: gopinadhan.kalon@iitgn.ac.in)

Contents:

Supplementary Figures:

Supplementary notes:

Supplementary tables:

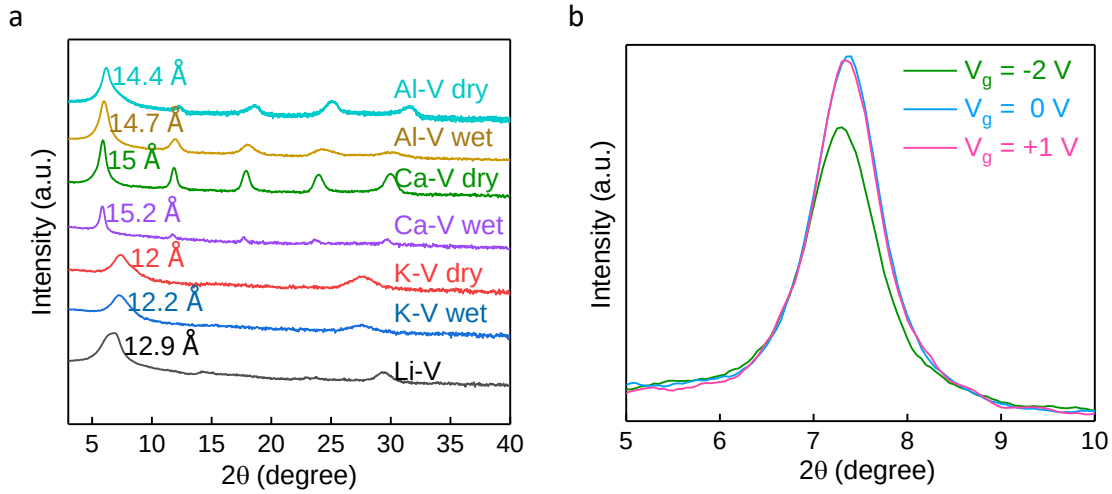

Supplementary Figure 1. X-ray diffraction (XRD) analysis of the cation-exchanged vermiculite membranes. a X-ray diffraction pattern of the Li-V, K-V, Ca-V, and Al-V membranes in both dry and wet state. The interlayer spacing is ~12 Å for K- V and Li-V membranes, and for Ca-V and Al-V membranes, it is ~15 Å. **b** In-situ X-ray diffraction pattern of the K-V device with various applied V_g at a solution concentration of 1000 mM KCl. We varied V_g from -2 V to 1 V and a solution of 1000 mM KCl concentration was used, which mimic our transport measurement conditions. It is observed from the XRD data that when V_g = 0 V, the intense peak of K-V is at 7.38˚ which changes to 7.29˚ at a V_g of -2 V. The estimated d-spacing of K-V membrane changes very little from 12 Å to 12.1 Å, a net change of 0.1 Å. It confirms that the interlayer spacing is not affected by gate voltage.

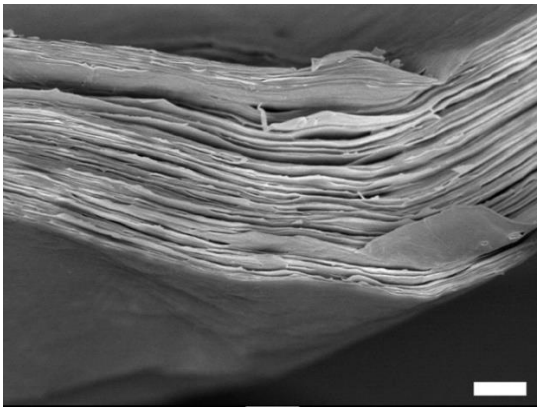

Supplementary Figure 2. Scanning electron microscopy (SEM) characterization of vermiculite membrane. Cross-sectional image of the K-V membrane shows laminated structure with thickness ~3.5 µm. The scale bar is 1 µm.

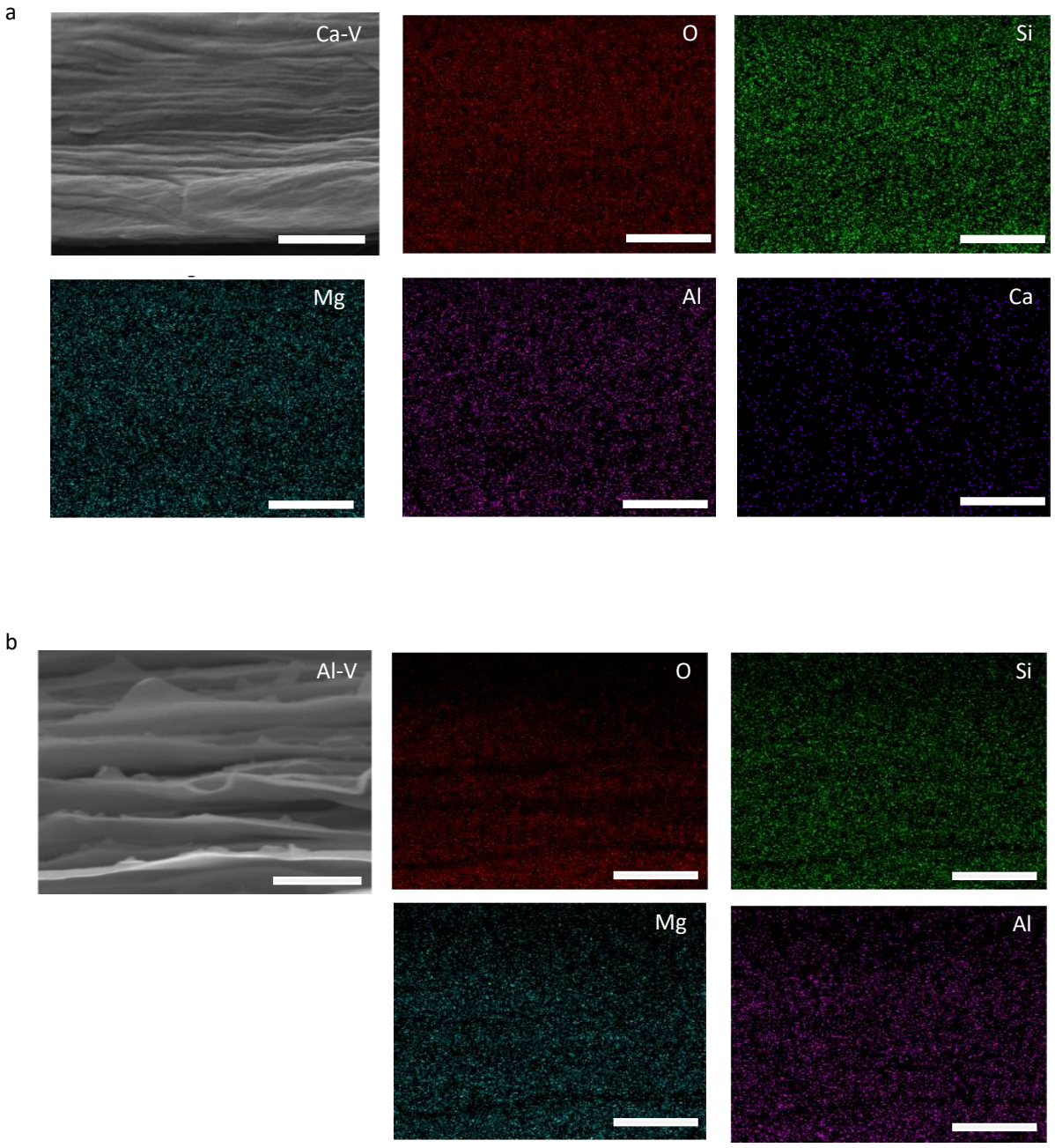

Supplementary Figure 3. Cross-sectional energy dispersive (EDS) elemental mapping of Ca-V and Al-V membranes. The scale bar represents 1 µm. From the EDS mapping, we found that the main elements present are O, Si, Mg and Al. **a.** For Ca-V membranes, intercalant Ca is also detected. **b.** In Al-V membranes, the signal arising from the intercalant Al is merged with signal from the intrinsic Al, so no separate detection is possible.

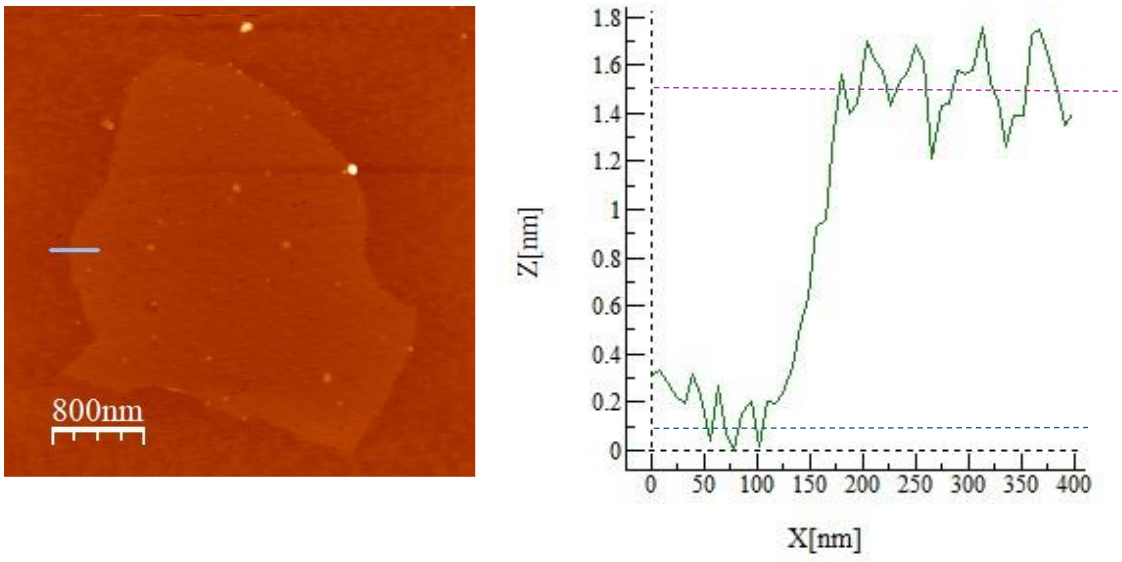

Supplementary Figure 4. Atomic force microscopy (AFM) image of the vermiculite. AFM image of monolayer vermiculite laminate with a flake size of ~2 µm. The flake sizes are typically in the range 1-3 µm. The height profile (the right image) provides a thickness of 14 Å for single layer vermiculite. Mica-like structure adsorbs 1 or 2 layers of water molecules on its surface and also host intercalated ions on its surface. This results in a slightly larger thickness of 14 Å instead of 9.6 Å.

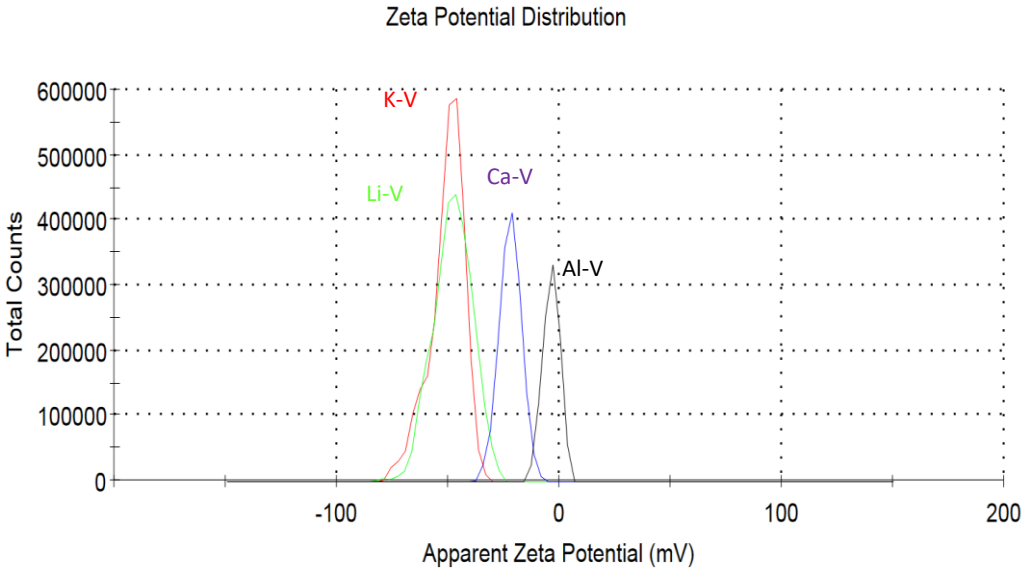

Supplementary Figure 5. Zeta potential characterization of cation-exchanged vermiculite laminates. Zeta potential measurement of the dispersed vermiculite flake solution with Li^+, K^+, Ca^{2+} and Al^{3+} intercalant is displayed. The concentration of the dispersed solution was 1 mg/mL in deionized water (DI). We measured the zeta potential in membrane as well as in dispersed forms and in both cases, the zeta potential is found to be similar. With increase in valence of the exchanged cation in vermiculite, the zeta potential is found to decrease.

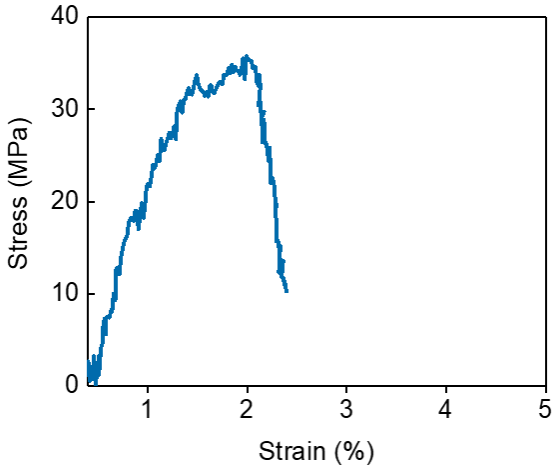

Supplementary Figure 6. Mechanical strength analysis of the vermiculite membrane. The tensile strength of vermiculite is approximately 35 MPa, with a fracture strain of about 2%. This indicates that vermiculite membranes are flexible and suitable for use in aqueous conditions.

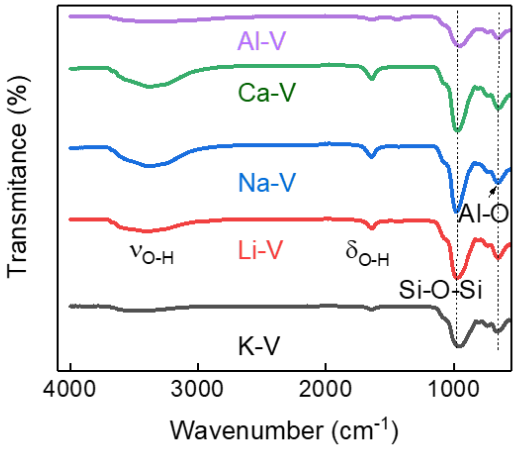

Supplementary Figure 7. FTIR analysis of the different intercalated membranes. The broad absorption peak at 3360 cm^{-1} and 1643 cm^{-1} indicates stretching vibration and bending vibrations of the -OH groups. The absorbance peak at 970 cm^{-1} is ascribed to the asymmetric stretching vibration of the Si-O-Si. Two peaks at 735 cm^{-1} and 652 cm^{-1} can be attributed to the Al-O-Al and M-O-Si (Mg, Al, Fe) bonds, respectively.

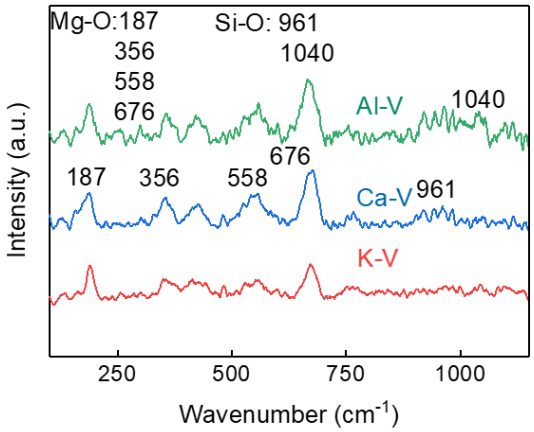

Supplementary Figure 8. Raman spectra of the K-V, Ca-V and Al-V membranes. The spectra show the characteristic peak of Mg-O/Al-O at positions 187, 356, 558 and 676 cm^{-1} and Si-O at 961 cm^{-1} and 1040 cm^{-1}, thus confirming the compositional aspect of magnesium aluminosilicate.

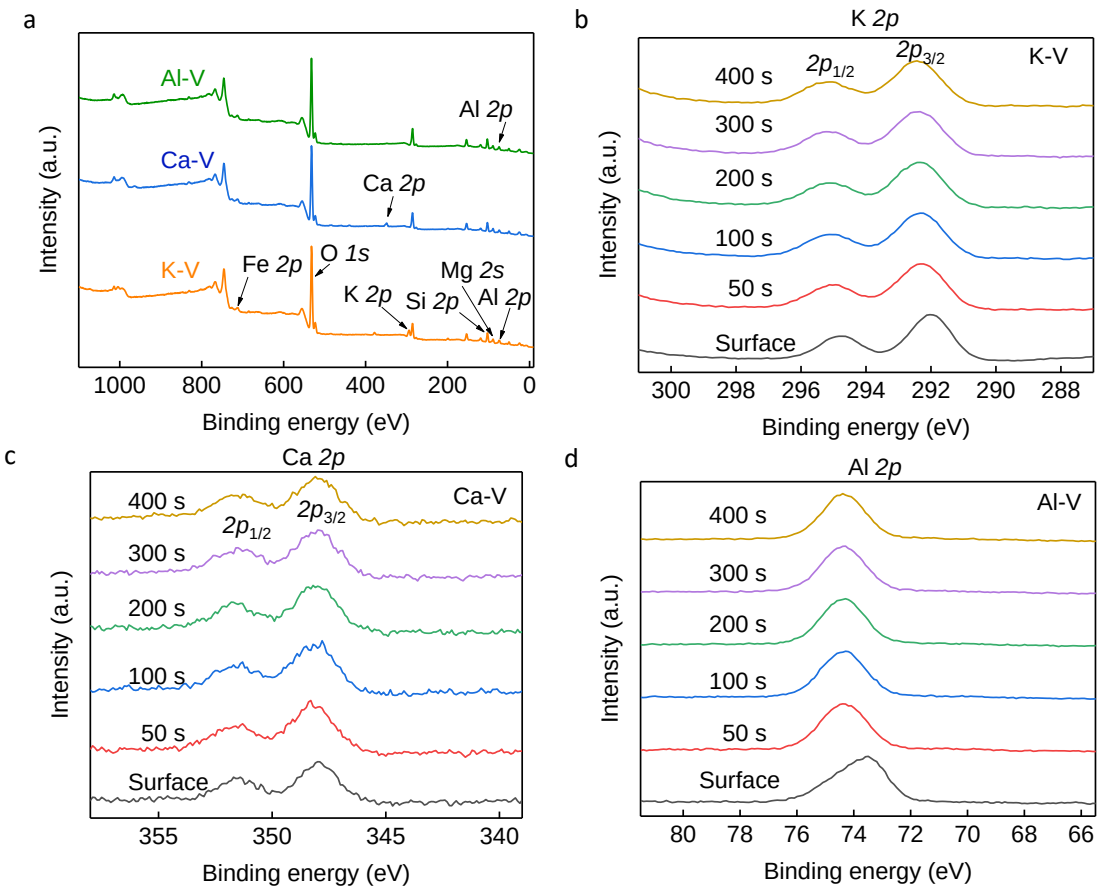

Supplementary Figure 9. XPS survey scan and depth analysis of the cation-intercalated vermiculite membranes. a XPS survey spectrum of K-V, Ca-V and Al-V membranes. It displays common elements present in the intercalated membrane such as O, Si, Mg and Al. Additionally, K, Ca and Al (merge with the intrinsic Al) signals are detected from K-V, Ca-V and Al-V membranes respectively, which confirms the successful intercalation of the cations inside vermiculite. **b** Depth profile scan of K-V membrane indicates the presence of K inside deeper layers of the membrane with uniform distribution. **c** Depth profile scan of Ca-V membrane confirming the presence of Ca inside the layers and its uniform distribution. **d** Depth profile scan of Al-V membrane indicates the presence of Al across the membrane and Al is uniformly distributed. Note that we could not distinguish the intercalated Al ion and the Al present in the tetrahedral sites.

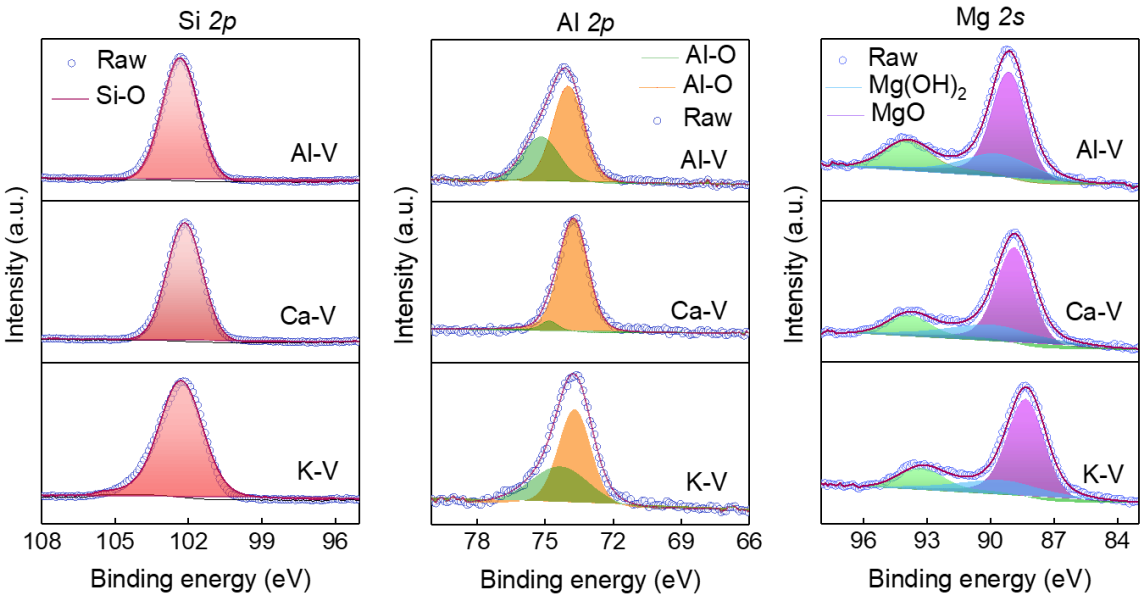

Supplementary Figure 10. X-ray photoelectron spectroscopy (XPS) studies of intrinsic elements of vermiculite, Si, Al and Mg (O 1s is given in the main text). Si 2p spectrum shows a peak at 102.3 eV for K-V and Ca-V membranes corresponding to Si-O. For Al-V membranes, Si 2p peak shows a slight shift towards higher binding energy side when compared to K-V (or Ca-V) membranes, which could be a result of increased ionicity due to intercalant Al^{3+}. For K-V sample, Al 2p peak at 73.7 eV corresponds to tetrahedral Al ($^{[4]}$Al) and higher binding energy peak of 74.4 eV corresponding to the octahedral Al ($^{[6]}$Al) [Ref.[1,2]]. The Al 2p peak being shifted towards higher binding energy side for Ca-V and Al-V samples. Mg 2s spectrum of K-V membranes shows Mg-O peak at 88.3 eV whereas the broad peak can be ascribed to $Mg(OH)_2$ [Ref. [3]]. These peaks are also observed in the case of Ca-V and Al-V membranes.

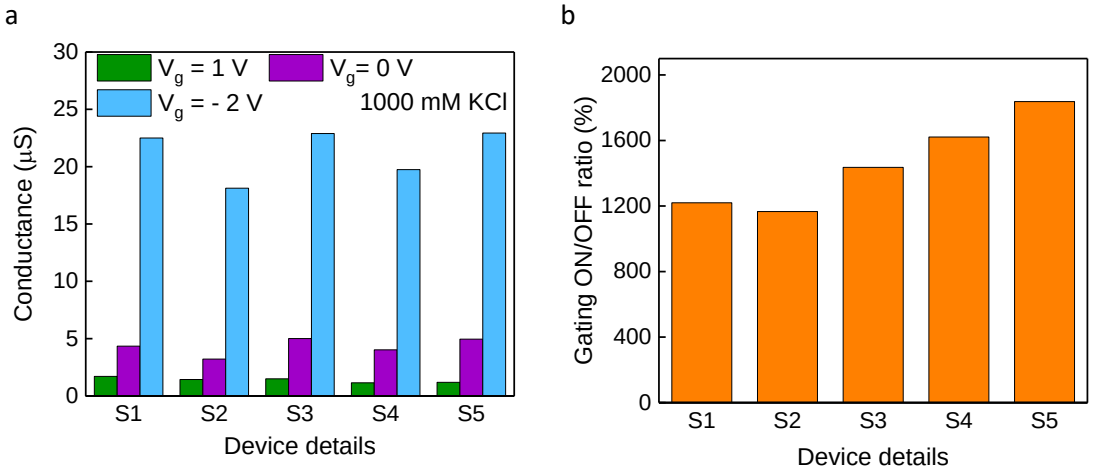

Supplementary Figure 11. Repeatability and reproducibility of several voltage-gated K-V devices. a Conductance of 5 different samples at V_g = +1 V, 0 V and -2 V for 1000 mM KCl. **b** The gating ON/OFF ratio estimated from figure a, for the extreme gate voltages, is displayed for several samples. We observed that most of our devices were stable and showed a similar behavior.

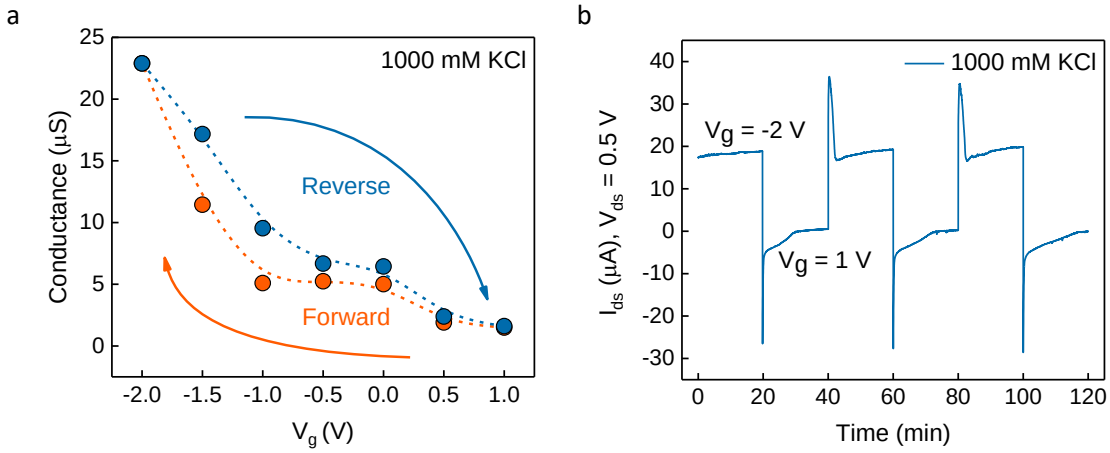

Supplementary Figure 12. Reversible modulation of conductance for 1000 mM KCl in K-V laminates. a Conductance change for 1000 mM KCl with gate voltages; the arrow represents the direction of the gate potential applied to the sample. The doted lines are a guide for the eye. This clearly shows that the device is stable, and at high concentration, we could tune the conductance efficiently. **b** Multicycle ionic current (I_{ds}) measurements at V_g = -2 V and 1 V with V_{ds} = 0.5 V shows the reversible modulation.

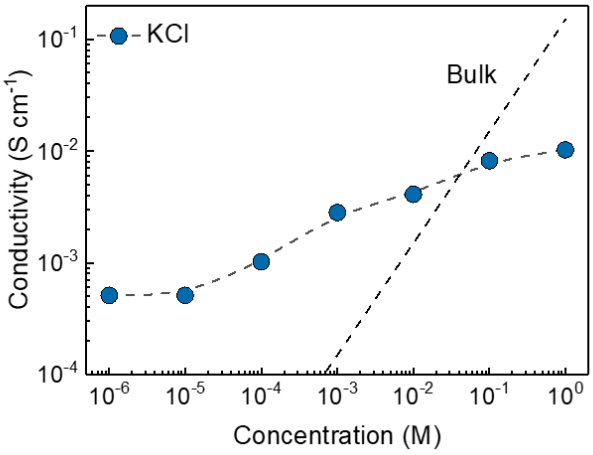

Supplementary Figure 13. Concentration-dependent conductivity data of K-V laminates. The measured conductance is plotted as a function of KCl concentration. The dotted line is a guide for the eye.

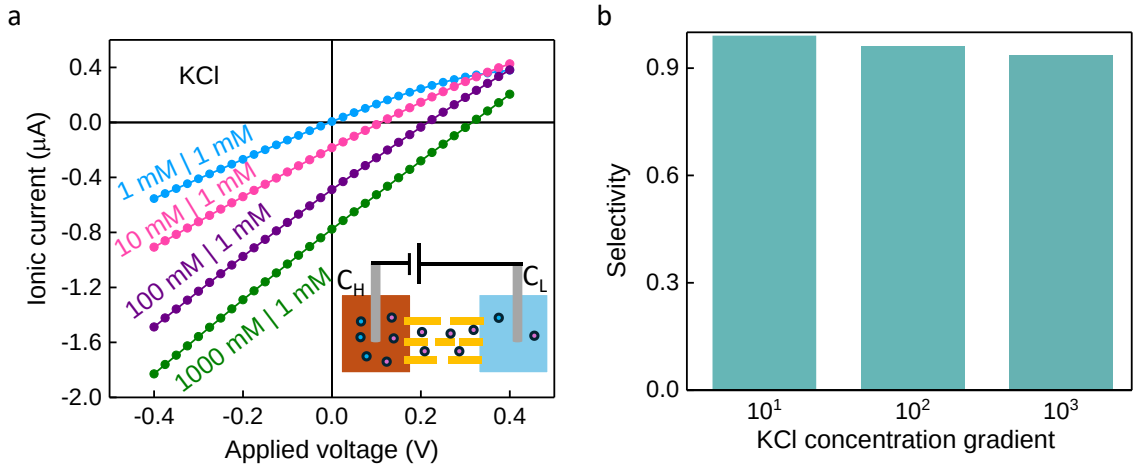

Supplementary Figure 14. Diffusion studies of K-V sample. a The ionic current as a function of applied potential without subtracting the redox potential of the electrodes. Inset: schematic of the diffusion measurement setup. **b** Ion selectivity with different KCl concentration gradients.

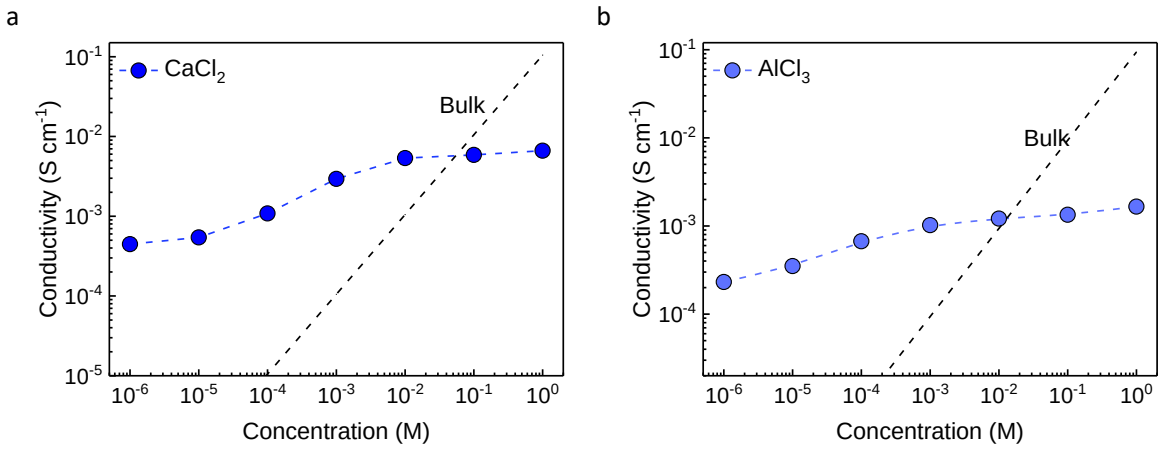

Supplementary Figure 15. Conductivity variation with concentration. a Ca-V laminate with $CaCl_2$ solution. **b** Al-V laminates with $AlCl_3$ solution. The dotted line is a guide for the eye.

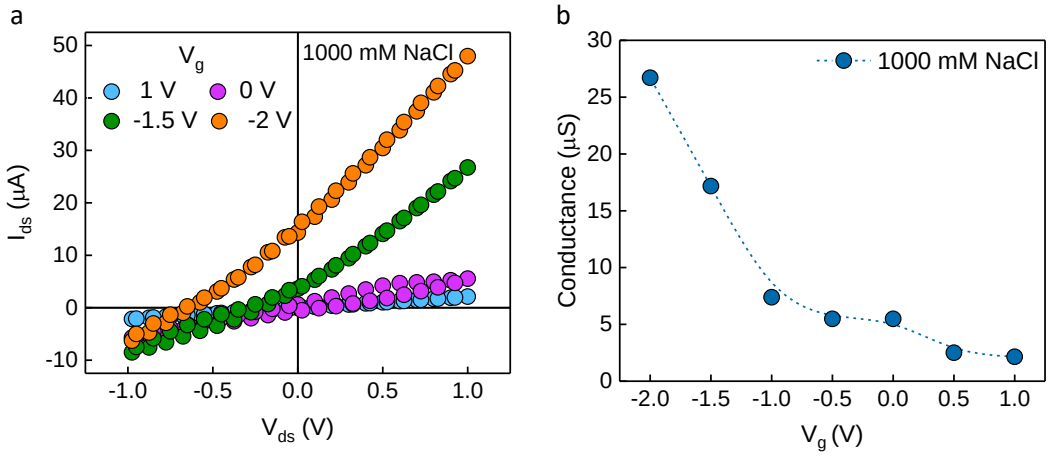

Supplementary Figure 16. **Voltage gated ion transport through Na-V membranes with 1000 mM NaCl**. **a** Modulation of ionic current, I_{ds} with different V_g from -2 V to 1 V with a step size of 0.5 V. The NaCl solution concentration is 1000 mM. **b** Variation of conductance with gate voltage (V_g) at a concentration of 1000 mM NaCl. The gating ON/OFF ratio is found to be ~1100%, slightly smaller than KCl for the same concentration.

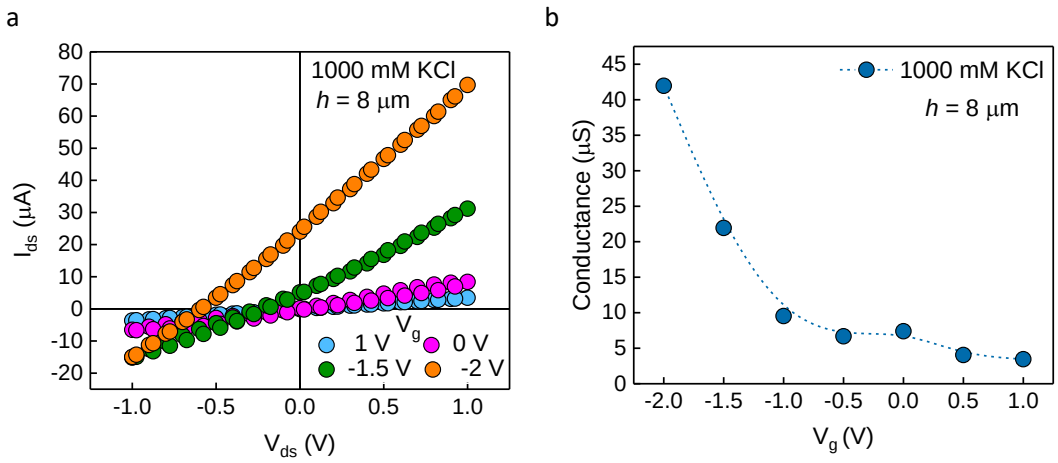

Supplementary Figure 17. **Voltage gated modulation of KCl ion transport through K-V membrane of thickness, *h* = 8 µm at a concentration of 1000 mM**. **a** Modulation of ionic current, I_{ds} with different V_g at 1000 mM KCl. **b** Conductance variation with different V_g at a concentration of 1000 mM KCl. The overall ionic conductance is higher in this case when compared to ***h*** = 3.5 µm. However, the gating ON/OFF ratio is found to be ~1100%, slightly smaller than ***h*** = 3.5 µm.

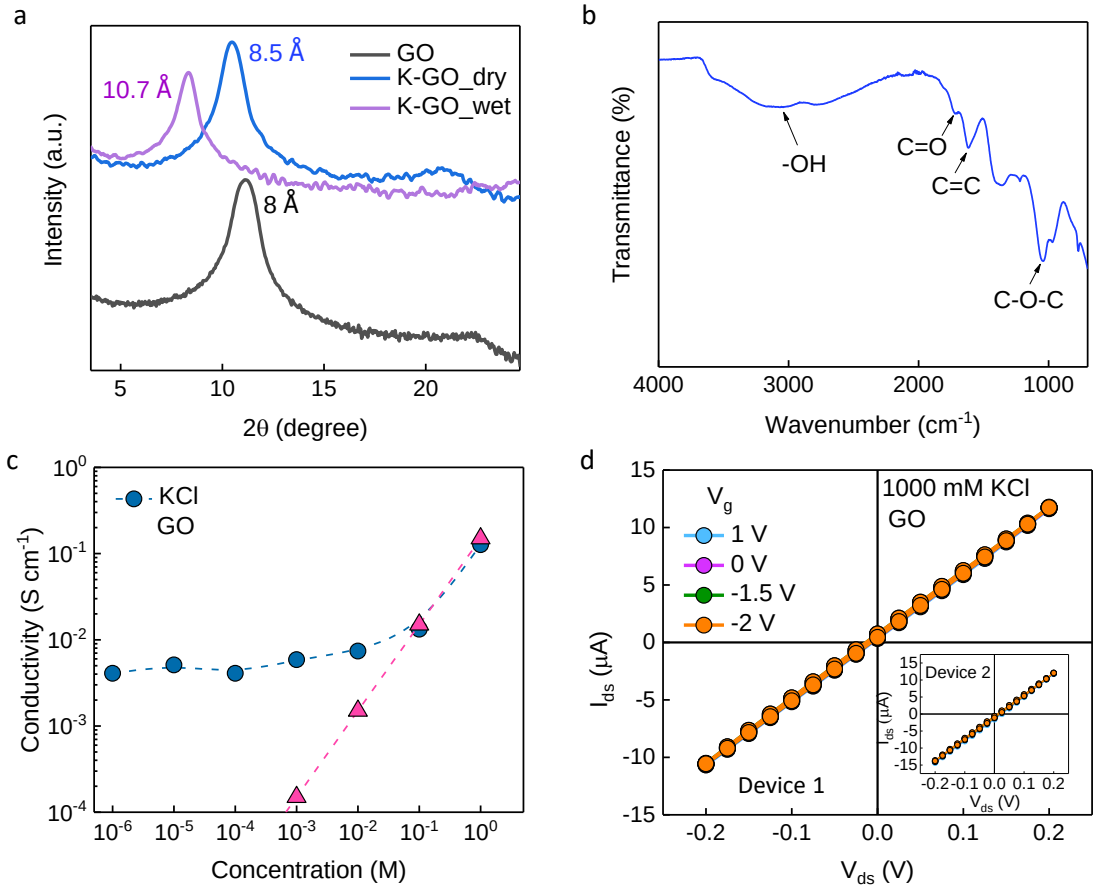

Supplementary Figure 18. Characterization and gated ion transport studies through the GO sample **a** XRD studies of GO, K-intercalated GO in wet and dry conditions**. b** FTIR studies of the GO sample show the characteristic peaks of -OH, C=C, C=O, and C-O-C**. c** Conductivity vs. concentration characteristics (represented as blue circles) of the GO sample with KCl salt solution. Bulk conductivity data (represented as pink triangles) is also provided for easy reference. **d** V_{ds}-I_{ds} characteristics at 1000 mM KCl for a GO sample (device 1) with different V_g values from -2 V to 1 V. Inset shows the data obtained from another device (device 2) with similar applied V_g as device 1.

Supplementary Note 1: Surface charge density calculation

The surface charge density of vermiculite layer is calculated from the measured zeta potential employing Gouy-Chapman equation;

$$\sigma = -\frac{\varepsilon_0\ \varepsilon_r \xi}{\lambda_d}\left(\frac{\sinh\left(\frac{F\xi}{2RT}\right)}{\frac{F\xi}{2RT}}\right) \qquad \text{Supplementary Equation (1)}$$

where ε_r is the dielectric constant, ε_0 is the permittivity of the free space, λ_d is the Debye length, F is the Faraday constant, R is the gas constant, T is the temperature and ξ is the zeta potential. The surface charge density is found to be ~-4 mC/m^2 for K-V membranes, assuming ε_r = 80 and C = 1 mM. The surface charge density for Ca-V and Al-V are ~-1.6 mC/m^2 and ~-0.3 mC/m^2.

Supplementary Note 2: Diffusion studies

In order to determine the ion selectivity of the membranes, we have carried out drift-diffusion studies through our in-plane K-V devices. The same voltage-gated membrane device was placed in the middle separating two reservoirs. The reservoirs were filled with various salt solutions such that concentration gradients of 10, 100, and 1000 were established. For this, we fixed the concentration of one reservoir to 1 mM and varied the concentration of the second reservoir from 10 mM to 1000 mM. Two home-made Ag/AgCl electrodes were used to measure the *I-V*'s.

It is known that electrodes placed in different concentrations produce an additional voltage known as the redox potential V_{redox}, and can be calculated from the equation given below[4],

$$V_{redox} = \frac{k_B T}{e}\ln\left(\frac{\gamma_H C_H}{\gamma_L C_L}\right) \qquad \text{Supplementary Equation (2)}$$

Where γ_H and γ_L are the mean activity co-efficient of ions at high and low salt concentrations, which depends on the type of salt used and their concentration. The actual membrane potential or diffusion potential, V_{diff} in the case of Ag/AgCl electrodes can be obtained after deducting the redox potential from the measured potential ($V_{measured}$).

$$V_{diff} = V_{measured} - V_{redox} \qquad \text{Supplementary Equation (3)}$$

The selectivity is calculated from the Nernst potential as follows,

$$V_{diff} = S\ \frac{RT}{zF}\ln\left(\frac{\gamma_H C_H}{\gamma_L C_L}\right) \qquad \text{Supplementary Equation (4)}$$

Where R, T, and F are gas constant, temperature, and Faraday constant respectively, z is the ion valence. Here, S = t_+ - t_-, where t_+, and t_- are the cationic and anionic transference numbers, respectively. Ion selectivity, S = 1, implies a perfectly cation-selective membrane, and S = 0 means the absence of any ion selectivity. We found that S = 0.96 for our K-V device from the above formula. This shows that K-V laminates are near ideal cationic membranes that only allow cations to transport even at high chloride concentrations of 1000 mM.

Supplementary Note 3: Fabrication of graphene oxide membrane:

Materials

Graphite, $KMnO_4$, H_2O_2 (35 wt%), HCl (34 wt%), potassium chloride (KCl) (> 99%), and PVDF (0.22 µm pore size) were purchased from Sigma Aldrich.

Fabrication of GO laminates

The synthesis of graphene oxide (GO) was carried out utilizing a modified Hummers' method. Initially, 1 g of graphite flakes was mixed with 35 mL of concentrated sulfuric acid (H_2SO_4) in a beaker. This mixture was subjected to stirring at 500 rpm using a magnetic stirrer, while ensuring that the temperature remained below 10°C. Subsequently, 3 g of potassium permanganate ($KMnO_4$) was incrementally added to the beaker, resulting in a color change of the solution to greenish. This mixture was stirred continuously for a duration of 6 hours. Following this period, 25 mL of deionized (DI) water was added dropwise to the slurry to terminate the oxidation process, after which an additional 50 mL of DI water was added. This resulted in a shift of the solution's color from greenish to brownish, an indication of the formation of graphite oxide. After allowing the mixture to settle for 15 minutes, 5 mL of hydrogen peroxide (H_2O_2) was added, which caused the color of the solution to return to a greenish tone. To purify the resulting slurry, a hydrochloric acid (HCl) solution at 10 wt.% was used, followed by centrifugation at 8000 rpm. This process was further continued with DI water until the pH of the solution reaches 7. The resultant GO powder was obtained by freeze-drying the slurry for 72 to 90 hours. A solution with a concentration of 1 mg/mL of GO was prepared using DI water as the solvent; this involved sonicating the mixture for 1 hour and subsequently centrifuging at 5000 rpm to isolate the supernatant for membrane preparation. Polyvinylidene fluoride (PVDF) with pore size of 0.22 µm was utilized as the supporting membrane during the fabrication process through vacuum filtration. After drying the GO membrane on PVDF, it was observed that the membrane easily peels off from the PVDF support. These membranes were further used for the characterization and ion transport studies.

XRD and FTIR studies:

The XRD of GO shows a d-spacing of 8 Å and a transport height of 4.6 Å after deducing the single-layer thickness of graphene (0.34 nm) (Supplementary Fig. 18a). The d-spacing of as-prepared GO is consistent with earlier reports[6]. The KCl (1 M) dipped GO membrane shows a d-spacing of 8.5 Å and 10.7 Å, respectively, in dry and wet conditions. Since our measured devices are in an aqueous solution, the transport height for the KCl-dipped GO membrane is 7.3 Å. We carried out an FTIR study of the GO sample, which shows characteristic peaks of -OH at 3088 cm^{-1}, C=C at 1617 cm^{-1}, C=O at 1720 cm^{-1}, and C-O-C at 1040 cm^{-1}, matching with literature values (Supplementary Fig. 18b)[7]. We performed ion transport studies through the as-fabricated membrane, and the conductivity vs. concentration characteristics show that above 100 mM concentration, the transport is bulk-like. As the transport height is 7.3 Å, at 1000 mM concentration, the Debye layer does not overlap and gives a bulk conductance value (Supplementary Fig. 18c). Then we checked the effect of gating at 1000 mM KCl concentration, and the I-V results are displayed with different V_g values; the slope did not change, suggesting that the conductance is not influenced by a gate (Supplementary Fig. 18d).

Supplementary Table 1. Summary of gating ON/OFF ratio for different gated nanofluidic systems. Most of the studies were performed at dilute salt concentrations, and the large Debye screening length at these concentrations ensures that there is an electrostatic effect.

Material	Concentration	Transport height	Gate voltage (V_g)	Gating ON/OFF ratio (%)	Reference
GO	50 mM KCl	1.66 nm	-0.5 V to 0 V	~300 - 400	*Nature Nanotech* 13, 685 (2018)
MXene	10 mM KCl	0.7 nm	1 V to -1 V	<1000	*ACS Nano* 13, 11793 (2019)
Mesoporous silica nanotube aligned film	$[H^+]$ = 0.1 mM	<8 nm	-1 V to 1 V	~200	*Nature Mater* 7, 303 (2008)
rGO	0.2 M KCl	~0.3 nm	0 V to -1.2 V	Off to On	Science 372, 501 (2021)
Silica nano channel	1 mM KCl	35 nm	-20 V to 20 V	~130	Nano Lett. 5, 943 (2005)
Vermiculite	1000 mM KCl	~0.3 nm	-2 V to 1 V	1400	This work

Supplementary Table 2. Activity coefficients and ion selectivity of K-V membranes in KCl solutions. The parameters ion selectivity, S and activity coefficient, γ with KCl solution is provided for K-V membranes at different concentration gradients. The redox potential is estimated from the Nernst equation and provided in the table at different concentration gradients. These measurements were performed at a temperature of 298 K.

Concentration gradient (KCl)	$V_{measured}$ (mV)	V_{redox} (mV)	V_{diff} (mV)	$\frac{\gamma_H}{\gamma_L}$ $(Ref.^5)$	S
10	114.20	57.37	56.83	0.933	0.9906
100	220.40	112.40	108	0.795	0.9608
1000	319.90	165.37	154.53	0.625	0.9345

References:

1. Barr, T. L., Seal, S., Wozniak, K. & Klinowski, J. ESCA studies of the coordination state of aluminium in oxide environments. *J. Chem. Soc. Faraday Trans.* **93**, 181–186 (1997).

2. Kądziołka-Gaweł, M., Czaja, M., Dulski, M., Krzykawski, T. & Szubka, M. Impact of high temperatures on aluminoceladonite studied by Mössbauer, Raman, X-ray diffraction and X-ray photoelectron spectroscopy. *Mineral. Petrol.* **115**, 431–444 (2021).
3. Le Febvrier, A., Jensen, J. & Eklund, P. Wet-cleaning of MgO(001): modification of surface chemistry and effects on thin film growth investigated by x-ray photoelectron spectroscopy and time-of-flight secondary ion mass spectroscopy. *J. Vac. Sci. Technol. A* **35**, 021407 (2017).
4. Guo, W. *et al.* Energy harvesting with single-ion-selective nanopores: a concentration-gradient-driven nanofluidic power source. *Adv. Funct. Mater.* **20**, 1339–1344 (2010).
5. CRC Handbook of Chemistry and Physics 95th Edition.pdf.
6. Chen, L. *et al.* Ion sieving in graphene oxide membranes via cationic control of interlayer spacing. *Nature* **550**, 380–383 (2017).
7. Emiru, T. F. & and Ayele, D. W. Controlled synthesis, characterization and reduction of graphene oxide: A convenient method for large scale production. *Egypt. J. Basic Appl. Sci.* **4**, 74–79 (2017).